



## Oxidation and erosion behaviour of SiC-HfC multilayered composite

Branko Matović<sup>1,\*</sup>, Vesna Maksimović<sup>1</sup>, Dušan Bučevac<sup>1</sup>, Jelena Pantić<sup>1</sup>, Jelena Luković<sup>1</sup>, Tatjana Volkov-Husović<sup>2</sup>, Devendraprakash Gautam<sup>3</sup>

<sup>1</sup>*Vinča Institute of Nuclear Sciences, University of Belgrade, P. O. Box 522, Belgrade, Serbia*

<sup>2</sup>*Faculty of Technology and Metallurgy, Metallurgical Engineering Department, University of Belgrade, Karnegijeva 4, Belgrade, Serbia*

<sup>3</sup>*Nanoparticle Process Technology, Department of Engineering Sciences, University of Duisburg-Essen, Lotharstrasse 1, MA 343, D-47057, Duisburg, Germany*

Received 13 January 2014; Received in revised form 26 March 2014; Accepted 28 March 2014

### Abstract

*The fabrication of SiC-HfC ceramic composite via self-propagating high-temperature synthesis and simultaneous consolidation was investigated. Dense composite consisting of alternating layers of SiC and HfC was obtained by spark plasma sintering of stack of SiC cloths covered by electrophoretically deposited HfO<sub>2</sub>. The deposited HfO<sub>2</sub> was converted into HfC during sintering. The obtained ceramics was characterized in terms of microstructure, cavitation resistance and oxidation resistance. It was shown that spark plasma sintering is effective way to preserve fibre-like mikrostructure of SiC. The obtained material showed good erosion resistance. The surface layer of HfC transformed to HfO<sub>2</sub> during oxidation of samples and protected SiC from further oxidation.*

**Keywords:** SiC, spark plasma sintering, corrosion, scanning electron microscopy, refractories

### I. Introduction

Silicon carbide (SiC) possesses a good combination of thermo-mechanical and chemical properties which makes it one of the most useful materials for high-temperature structural application. SiC is the fourth hardest material with low thermal expansion coefficient, good thermal conductivity and high fracture strength which can be retained even at temperatures above 1000 °C. Its good thermal and chemical stability, excellent oxidation, corrosion and wear resistance and relatively good resistance to high neutron irradiation make SiC promising material for harsh environment [1–4]. It is believed that these properties can be exploited at even higher temperature, i.e., above 2000 °C if SiC is protected by ultra-high temperature ceramics (UHTCs) [5,6]. UHTCs are normally transition metal carbides such as ZrC, HfC, TaC and NbC which can withstand extremely high temperatures (>3000 °C), high pressure and high speed particle erosion owing to their high melt-

ing point, high hardness and strength at elevated temperatures [6–8]. Among these refractory metal carbides, HfC possesses the highest melting point of 3890 °C. Besides low vapour pressure [9], high hardness and strength at elevated temperature [10], HfC also possesses excellent chemical stability [11,12]. As far as structural application is concerned, the main disadvantage of HfC is its high density of 12.2 g/cm<sup>3</sup>. This value is almost four times higher than that of SiC and consequently the use of HfC components will considerably increase the overall weight of manufactured devices. It is believed that the combination of SiC and HfC will result in light composite material with good mechanical properties as well as oxidation resistance which can be used in extremely harsh environment. Namely, the high-temperature oxidation of HfC leads to formation of protective HfO<sub>2</sub> layer which also has a very high melting point of 2810 °C and relatively low vapour pressure [13]. Therefore, HfC coating/layer is expected to protect SiC as well as composite from evaporation, erosion and oxidation at ultra-high temperature.

Monolithic transition metal carbide-based UHTCs

\*Corresponding author: tel: +381 11 3408 753, fax: +381 11 3408 224, e-mail: [mato@vinca.rs](mailto:mato@vinca.rs)

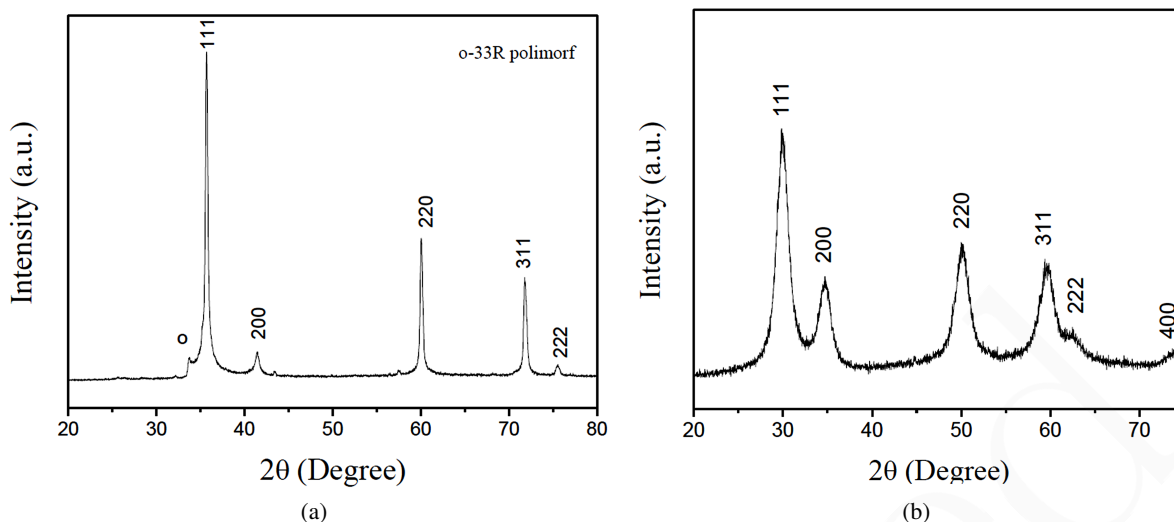


Figure 1. XRD patterns of SiC cloth (a) and Y doped  $\text{HfO}_2$  (b)

are typically processed by hot pressing (HP) or spark plasma sintering (SPS) of starting materials [14,15]. Moreover, composite ceramics such as SiC-HfC ceramics can be obtained by reactive synthesis starting from SiC and  $\text{HfO}_2$  powders and its simultaneous densification by HP or SPS. Pure  $\text{HfO}_2$  exhibits monoclinic crystal structure at room temperature, which transforms to tetragonal and cubic structure at elevated temperatures [16]. The volume expansion caused by the cubic to tetragonal to monoclinic transformation induces large internal thermal stresses, which normally result in cracking of pure  $\text{HfO}_2$  during cooling from high temperatures. It was found that the cracking is mainly caused by the stresses introduced by tetragonal to monoclinic transformation and therefore it would be essential to avoid formation of monoclinic  $\text{HfO}_2$ . Several studies have reported that the addition of oxides such as  $\text{MgO}$ ,  $\text{Y}_2\text{O}_3$  and  $\text{CaO}$  is an effective way to stabilize the tetragonal and/or cubic  $\text{HfO}_2$  [17,18]. The cubic phase of  $\text{HfO}_2$  has a very low thermal conductivity, which has led to its use as a thermal barrier coating in jet and diesel engines to allow operation at high temperatures [19].

In the present work, SiC-HfC layered composite was fabricated by employing self-propagating high-temperature reaction between SiC cloth and electrophoretically deposited 20 wt.% yttrium doped  $\text{HfO}_2$ . The stacks of hafnia covered SiC cloth were consolidated by SPS. The obtained ceramic composite was characterized in terms of microstructure, cavitation resistance and oxidation resistance.

## II. Materials and experimental techniques

Two-dimensionally plain-woven polycrystalline SiC fiber cloth (Tyrano SA, Ube Industries, Ltd., Japan) and 20 wt.% yttrium doped  $\text{HfO}_2$  nano-powders were used. XRD pattern of SiC cloth, presented in Fig. 1a, shows that the main phase is cubic SiC (3C polymorph) whereas the minor phase is 33R polymorph. The cloth

was cut into squares of 50 mm×50 mm. The polyethylene oxide (sizing agent) was removed from the cloth surface by immersion in hot distilled water for 15 min. Synthesis of 20 wt.% yttrium doped  $\text{HfO}_2$  was described in detail elsewhere [20]. A relatively large amount of yttrium was used in order to insure complete stabilization of the cubic phase of  $\text{HfO}_2$ . XRD pattern of  $\text{HfO}_2$  powder which confirms that the main phase is cubic is shown in Fig. 1b. The particle size of yttrium doped  $\text{HfO}_2$ , calculated from XRD pattern using Scherrer's method [21], lies in the nanometric range (~6 nm) which makes the deposited hafnia powder very reactive.

SiC cloth was coated with yttrium doped  $\text{HfO}_2$  powder by electrophoretic deposition using  $\text{HfO}_2$  suspension under an applied voltage of 3 V for 30 min. The concentration of colloidal  $\text{HfO}_2$  suspension was adjusted to 0.1 wt.% whereas pH of the solution was adjusted to 7. The SiC fiber cloth as an anode and the graphite plate as a cathode were settled at the distance of 10 mm in the  $\text{HfO}_2$  suspension. The procedure was repeated 3 times. Prior to  $\text{HfO}_2$  deposition, the suspension of commercial colloidal graphite aqueous solution (Hitasol, Hitachi Powdered Metals, Co., Ltd., Japan) was also electrophoretically deposited on SiC cloth to provide better cohesion (adhesion) with  $\text{HfO}_2$  nanopowder. The concentration of colloidal graphite suspension was adjusted to 0.1 wt.% whereas pH of the solution was adjusted to 10 by adding a small amount of n-butylamine [22].

The  $\text{HfO}_2$  coated SiC cloths were stacked and heat-treated at 300 °C in air under a pressure of 0.02 MPa followed by SPS. The SPS equipment FCT HP D5 (FCT Systeme GmbH, Raunstein, Germany) was used for sintering. The mixture was loaded into the graphite die with an inner diameter of 20 mm. A boron nitride (BN) coated graphite foil was used to avoid the contact between the powder and the inner surface of the die. The sample was heated-up by a pulsed electric current from room temperature to 1800 °C with a heating rate

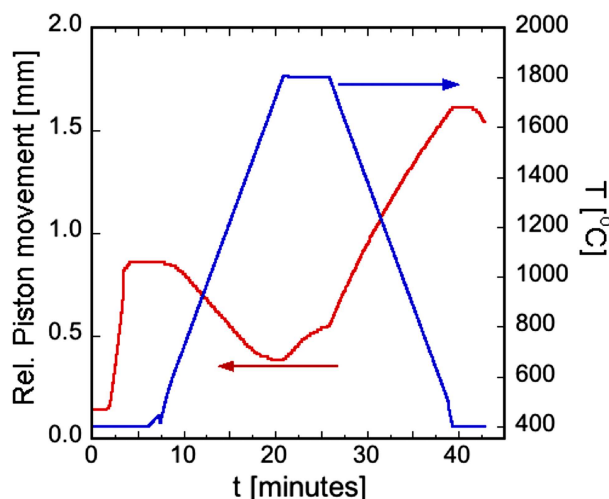


Figure 2. Variation of relative piston movement and temperature with time during SPS process

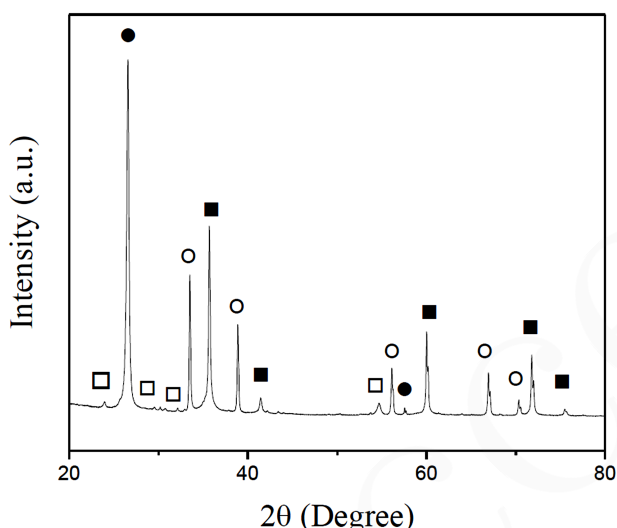


Figure 3. Room temperature XRD pattern of SPS treated materials, ■ - SiC, □ -  $Y_2SiO_5$ , ● - C, ○ - HfC

of 100 °C/min. The sample was held for 5 minutes at 1800 °C. It was cooled down to 500 °C with a rate of 100 °C/min and further to room temperature by natural cooling. A pressure of 35 MPa was applied on the sample over the complete heating-cooling cycle. The pressure on the specimen was released during natural cooling. The complete sintering was done under vacuum of  $\sim 100$  Pa (1 mbar). Cavitation wear was performed in order to study the erosion behaviour of obtained SPS sample. The fluid dynamic system of the cavitations erosion methodology used here to produce ultrasonic cavitations is explained in detail elsewhere [23]. The cavitation erosion testing was accomplished utilizing the recommended standard values: the frequency of the vibration was  $20 \pm 0.2$  kHz, the amplitude of the vibration at the top of the transformer was  $50 \pm 2$   $\mu$ m, the gap between the test specimen and the transformer was 5.0 mm, the temperature of water in the bath was  $25 \pm 1$  °C. These parameters were controlled throughout the testing process [24–27].

The evaluation of the mass losses of the test specimen was done on an analytical balance with an accuracy of  $\pm 0.1$  mg. The specimen was subjected to the fluid for 150 minutes. The weight measurement was performed every 30 minutes. The sample obtained after SPS was cut and tested for its oxidation stability at various temperatures under static ambient atmosphere for 4 h. The oxidation experiments at 1350, 1450 and 1550 °C were performed in a horizontal alumina tube furnace.

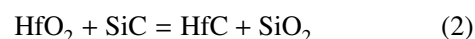
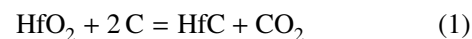
X-ray diffraction patterns were obtained on a Siemens D-500 XRD powder diffractometer with  $CuK_{\alpha}$  radiation in conjunction with  $CuK_{\beta}$  nickel filter. The surface and cross-section of the sintered sample as well as its phase composition were analysed by VEGA TS 5130 mm TESCAN SEM/EDS equipment.

### III. Results and discussion

#### 3.1. Ceramics preparation

The variation of relative piston movement and temperature with the time is presented in Fig. 2. As mentioned, the fast increase in sample temperature from room temperature to 1800 °C was followed by 5 minutes long hold. Before heating started, a pressure of 35 MPa had been applied leading to the sample compression as seen from the increment in the value of relative piston movement. During the heating cycle at temperature of  $\sim 650$  °C, the value of piston movement decreases and finally reaches the lowest level at  $\sim 1800$  °C. The decrease in relative piston movement during heating cycle could be understood as a result of sample expansion due to the reaction between sample constituents namely,  $HfO_2$ , C and SiC (see Eqs. 1 and 2). Figure 2 shows that the piston movement increases steadily after the sample stayed for a minute at 1800 °C. It seems that the reaction between the sample constituents is almost complete after a minute. The following increase in relative piston movement, i.e., the sample compaction is believed to be the result of two processes. One is the elimination of an additional porosity which was introduced by the release of gaseous reaction products such as  $CO_2$ . The other is sintering which is normally followed by sample shrinkage.

The formation of HfC is approved by XRD pattern of SPS sample presented in Fig. 3. As can be seen, the principal phase after sintering is still cubic  $\beta$ -SiC which reveals that  $\beta$ -SiC  $\rightarrow$   $\alpha$ -SiC transformation did not take place. A very strong peak at  $2\theta = 28^\circ$  belongs to C phase whereas several low intensity peaks are ascribed to  $Y_2SiO_5$ . It is believed that HfC is obtained by a reaction between  $HfO_2$  and carbon or SiC phase according to reactions:



The obtained  $SiO_2$  probably reacted with yttrium

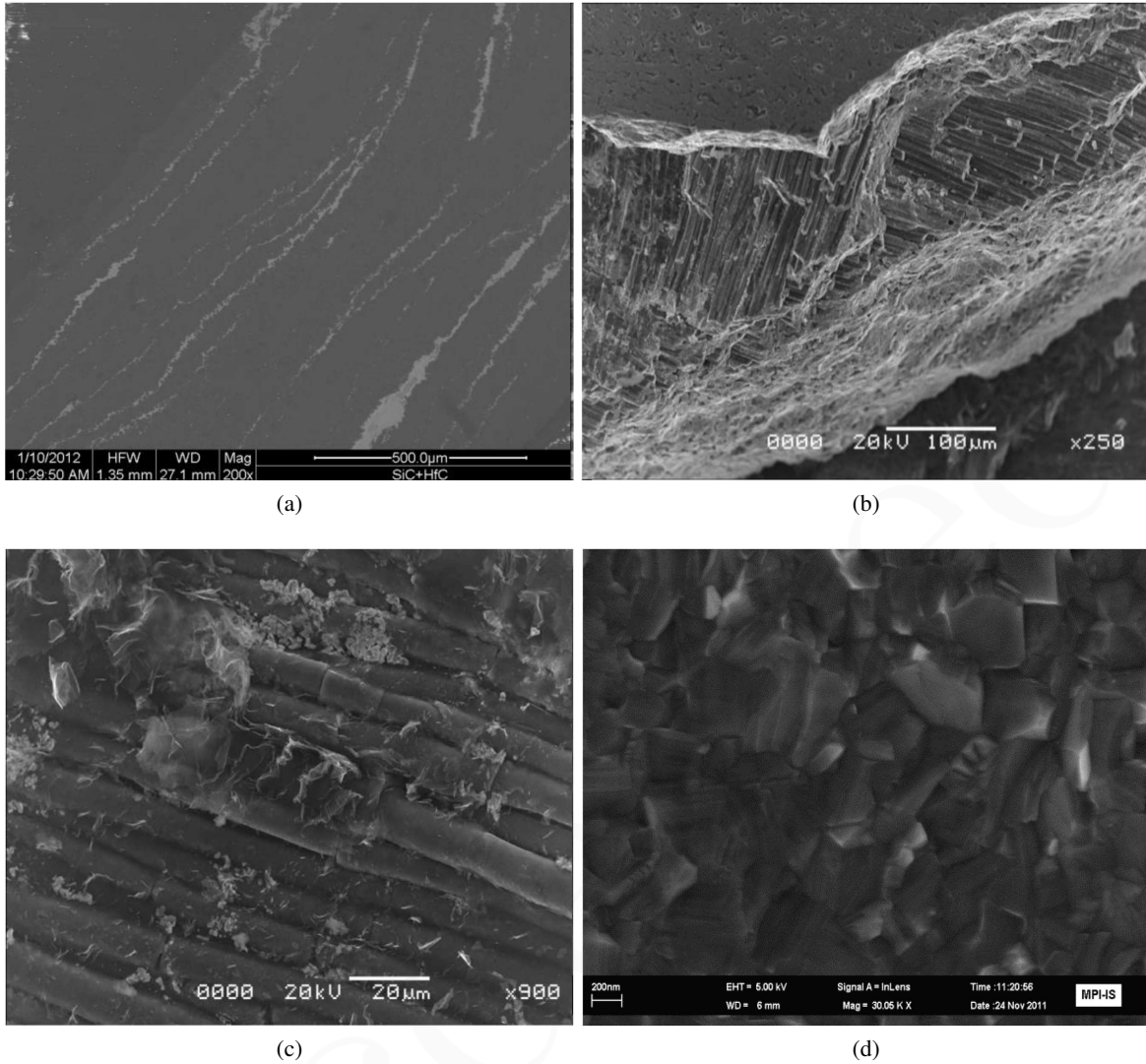


Figure 4. SEM micrographs of SPS material; (a) polished surface parallel to the pressing direction with EDS, (b) fracture surface, (c) SiC fibers and (d) cross-section of one SiC fiber

from yttrium doped  $\text{HfO}_2$  to form  $\text{Y}_2\text{SiO}_5$  as described by following reaction:



### 3.2. Microstructural feature of SPS sample

Figure 4a depicts polished surface of SPS sample which is parallel to the pressing direction. It is evident that SPS sintering of stack of  $\text{HfO}_2$  coated SiC cloths is an effective way to fabricate dense composite consisting of alternating thick layers of SiC (dark phase) and thin layers of HfC (bright phase). Energy dispersive spectroscopy (EDS) of the bright phase, given in Fig. 5, reveals the presence of Hf and C. The EDS spectrum also shows the small amount Y and O indicating the presence of  $\text{Y}_2\text{SiO}_5$ . A detail analysis of  $\text{Y}_2\text{SiO}_5$  phase was not conducted as the amount was very small. We believe that  $\text{Y}_2\text{SiO}_5$  exist as a thin layer between SiC and HfC. The reasoning for this was found in the fact that two constituents of  $\text{Y}_2\text{SiO}_5$ ,  $\text{SiO}_2$  and  $\text{Y}_2\text{O}_3$ , come from SiC

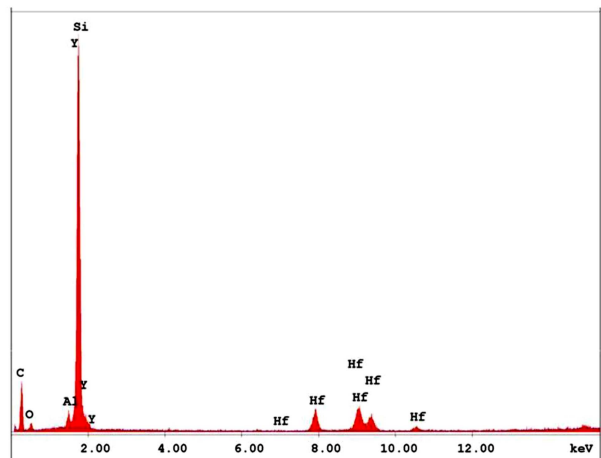


Figure 5. EDS spectrum of bright phase of SPS obtained SiC-HfC composite

and  $\text{HfO}_2$ , respectively. It is also important to stress that very high intensity of Si peak in EDS diagram comes

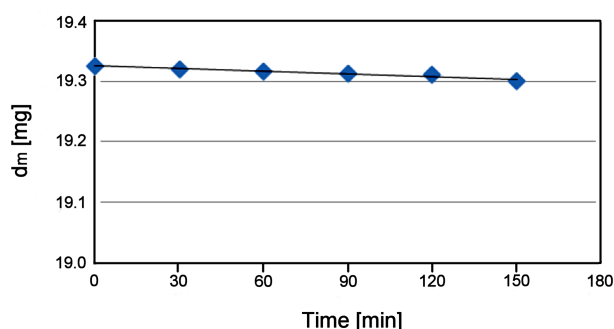


Figure 6. Mass loss during cavitation test of SPS obtained SiC-HfC composite

from surrounding SiC phase. The fracture surface of the composite is presented in Fig. 4b, which shows layers of differently oriented SiC fibers. Under high magnification (Fig. 4c), it can be seen that bamboo-like fibers have a radius less than 10  $\mu\text{m}$ . It is evident that the round cross section of the SiC fibers was maintained after SPS. The cross section of SiC fiber is presented in Fig. 4d, which reveals that SiC fiber consists of a regular SiC crystals with a size of about 200–300 nm.

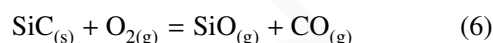
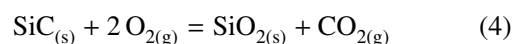
### 3.3. Cavitation erosion testing

The mass loss during the cavitation erosion experiment is illustrated in Fig. 6. The data show that the sample exhibited excellent resistance to the erosion cavitation. The mass loss was minimal. After 150 minutes of testing the mass loss was only 0.0024 g (0.12 wt.%). The optical microscopy analysis evidences that the surface of sample remains practically unchanged. These results were expected considering the results of the mass loss.

### 3.4. Oxidation mechanism of SiC-HfC

In general, the use of UHTC materials in air or combustion gases at elevated temperatures causes either active or passive oxidation. Active oxidation is normally followed by the weight loss due to formation of products which are immediately removed from the surface. How-

ever, passive oxidation is usually followed by a weight gain due to oxide layer formation. Although, there are several different oxidants such as  $\text{CO}_2$ ,  $\text{H}_2\text{O}$ ,  $\text{O}_2$ , only oxygen is taken into account in the present study. Thus, the main expected reactions which lead to the oxide formation are as follows:



Newly created  $\text{SiO}_2$  is expected to slow down the oxygen diffusion and therefore to protect SiC from fast oxidation. However,  $\text{HfO}_2$  has a much higher melting point than  $\text{SiO}_2$  and thus considered to be better protection when composite material is exposed to extremely high temperatures. The surface of SPS samples was not completely covered by HfC. There were areas, especially those close to the edge of samples, which were not covered by HfC due to the mechanical damage during fabrication. After oxidation, these areas have different chemical composition from the areas which were covered by HfC layer. Figure 7 shows the surface areas which were completely covered by HfC after oxidation at different temperatures. The sample oxidized at 1350  $^\circ\text{C}$  is covered by a porous  $\text{HfO}_2$  layer (Fig. 7a). The temperature of 1350  $^\circ\text{C}$  was sufficiently high to initiate sintering of  $\text{HfO}_2$  grains created by oxidation of HfC according to Eq. 7. Neck formation between  $\text{HfO}_2$  grains with a diameter of 1–2  $\mu\text{m}$  can be clearly seen in Fig. 7a. Further increase in temperature to 1450  $^\circ\text{C}$  promotes sintering of  $\text{HfO}_2$  grains. Figure 7b evidences that  $\text{HfO}_2$  layer becomes more compact, with large groups of firmly sintered grains. Finally, at high temperature such as 1550  $^\circ\text{C}$  the considerable shrinkage of  $\text{HfO}_2$  due

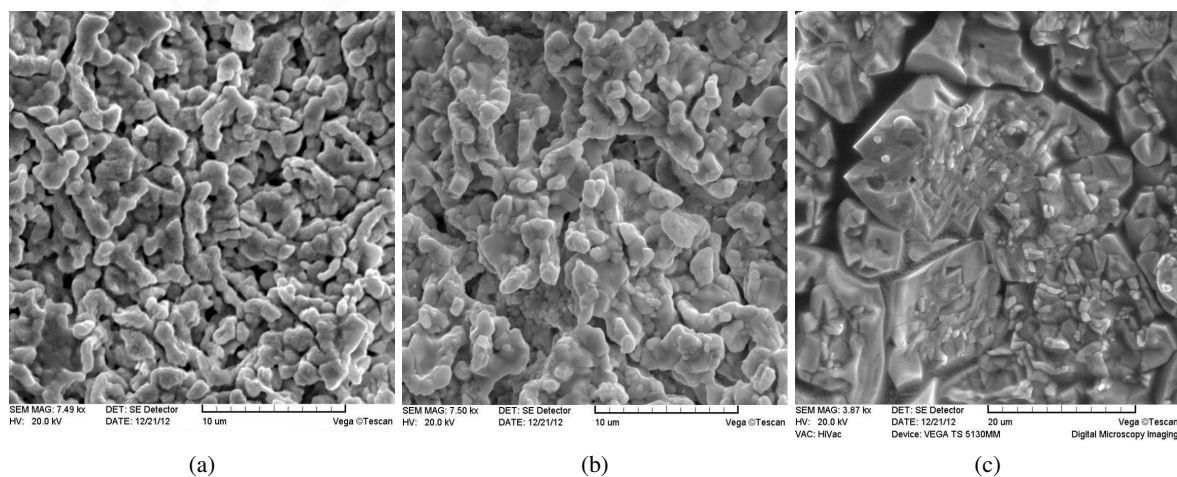


Figure 7. SEM micrographs of surface areas which were completely covered by HfC after four-hour long oxidation at: a) 1350  $^\circ\text{C}$ , b) 1450  $^\circ\text{C}$  and 1550  $^\circ\text{C}$

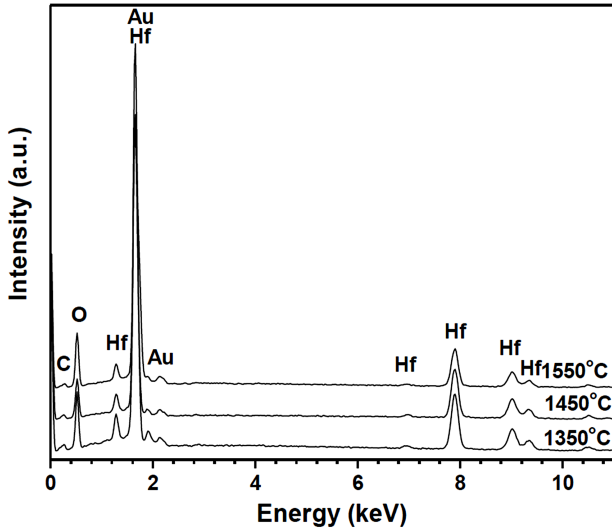
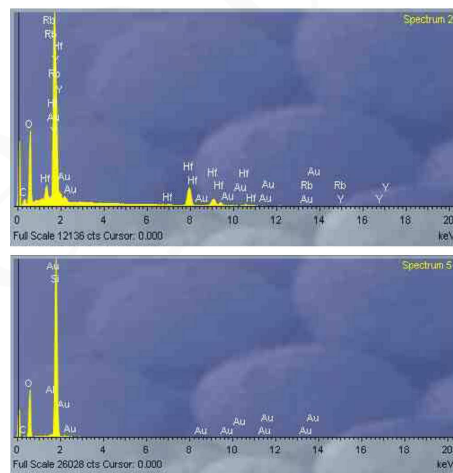
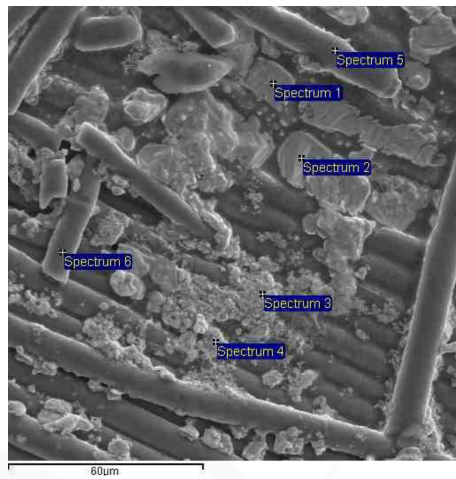
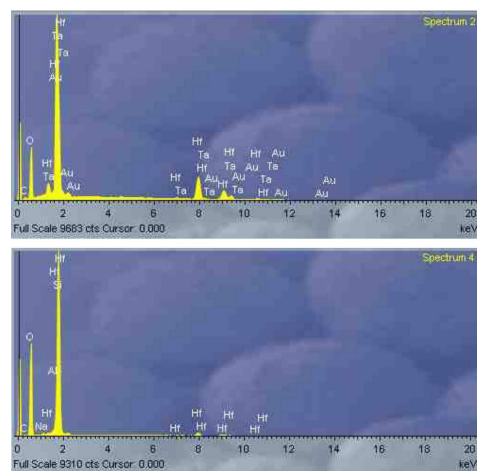
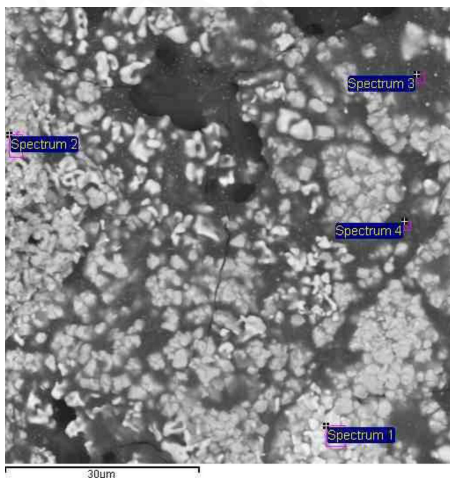


Figure 8. EDS spectra of surface areas which were completely covered by HfC after four-hour long oxidation at: a) 1350 °C, b) 1450 °C and 1550 °C

to sintering causes formation of large cracks in  $\text{HfO}_2$  layer (Fig. 7c). The cracking of oxide layer during extended oxidation is quite expected and very often inevitable. In general, the role of protective oxide layer is to slow down the oxidation (degradation) of protected material as much as possible. The important finding of this analysis is that SiC can be protected from excessive oxidation by  $\text{HfO}_2$  layer. The EDS spectra of surface of samples oxidized at different temperature given in Fig. 8 are almost the same indicating that newly formed surface layer is  $\text{HfO}_2$  regardless of oxidation temperature. Now it would be of interest to study the possible reaction between  $\text{HfO}_2$  and  $\text{SiO}_2$ , which are created during the oxidation of HfC and SiC, respectively. For this purpose the areas which are not completely covered by  $\text{HfO}_2$  were chosen as it was possible to study the contact between SiC and  $\text{HfO}_2$  by EDS and XRD analysis. The surface of sample oxidized at 1350 °C is presented in Fig. 9a. With the help of EDS analysis, it can be inferred that SiC fibres are coated as well as bonded with  $\text{SiO}_2$  glassy layer. The presence of  $\text{SiO}_2$  is expected knowing that SiC oxidizes above 1000 °C according to Eqs. 4–6.



(a)



(b)

Figure 9. SEM micrographs and EDS spectra of surface areas which were not completely covered by HfC after four-hour long oxidation at a) 1350 °C and b) 1550 °C

The bright phase consisting of Hf and O is HfO<sub>2</sub> which is formed by oxidation of HfC at ~600 °C (Eq. 7). The residual HfC was not found indicating that the oxidation of HfC is complete. As Fig. 9b reveals, the increase in oxidation temperature to 1550 °C leads to the formation of the dark phase consisting of Hf, O and Si (see EDS spectrum). The XRD analysis (not presented) confirms that this compound is hafnium silicate named hafnom (HfSiO<sub>4</sub>), which is formed by reaction between HfO<sub>2</sub> and SiO<sub>2</sub>:



At 1550 °C hafnom is in the form of viscous liquid which spreads out forming a compact layer with relatively homogeneously dispersed white phase of HfO<sub>2</sub> (see EDS spectrum). This layer has a better stability than silica glass and therefore exhibits a good protecting ability for UHTC material. The cracks, visible in Fig. 9b, are considered to be the result of volume shrinkage due to rapid cooling to the room temperature. The shrinkage generates a tensile residual stress at the sample surface, which promotes formation of cracks.

The weight gain (Table 1) can also confirm the passive oxidation, i.e., the ability of formed oxide layer to prevent oxygen diffusion into the material.

**Table 1. Weight change after oxidation at different temperature.**

Temperature [°C]	1350	1450	1550
Mass change [g]	+0.04	+0.08	+0.21

#### IV. Conclusions

Dense composite consisting of alternating layers of SiC and HfC was “in-situ” fabricated by spark plasma sintering of a stack of SiC cloths covered by electrophoretically deposited HfO<sub>2</sub>. The deposited HfO<sub>2</sub> was converted into HfC during sintering. The obtained material showed good erosion resistance. The surface layer of HfC transformed to HfO<sub>2</sub> during oxidation of samples which protected the composite from further oxidation.

**Acknowledgement:** This project was financially supported by the Ministry of Education and Science and Technological Development of Serbia (project number: III 45012).

#### References

1. D. Woodilla, M. Buonomo, I. Bar-On, “Elevated-temperature behaviour of high-strength silicon carbide”, *J. Am. Ceram. Soc.*, **76** (1993) 249–252.
2. H. Tanaka, “Silicon carbide powder and sintered materials”, *J. Ceram. Soc. Jpn.*, **119** (2011) 218–233.
3. B. Matović, T. Yano, “Chapter 3.1 - Silicon Carbide and Other Carbides”, pp. 225–244 in *From Stars to*

*the Advanced Ceramics Handbook of Advanced Ceramics* (Second Edition). Ed. Shigeyuki Somiya, Oxford, 2013.

4. H. Tanaka, T. Iseki, pp. 339–346 in: *Advanced Silicon Carbide Ceramics*, Edited by Japan Soc. Promo. Sci., The 124<sup>th</sup> Committee, Uchida Roukaku Publ., Tokyo, 2001.
5. E. Wuchina, E. Opila, M. Opeka, W. Fahrenholtz, I. Talmy, “UHTCs ultra-high temperature ceramic materials for extreme environment applications”, *Electrochem. Soc. Interface.*, **16** (2007) 30–36.
6. K. Upadhyaya, J.M. Yang, W. Hoffman, “Materials for ultrahigh temperature structural applications”, *Am. Ceram. Soc. Bull.*, **76** (1997) 51–56.
7. Y. Kumashiro, *Electric Refractory Materials*, Marcel Dekker, New York, 2000.
8. I.E. Campbell, E.M. Sherwood, *High-Temperature Materials and Technology*, Wiley, New York, 1967.
9. A. Sayir, “Carbon fiber reinforced hafnium carbide composite”, *J. Mater. Sci.*, **39** (2004) 5995–6003.
10. S.N. Karlsdottir, J.M. Halloran, “Rapid oxidation characterization of ultrahigh temperature ceramics”, *J. Am. Ceram. Soc.*, **90** (2007) 3233–3238.
11. S.R. Levine, “Evolution of ultra-high temperature ceramics for aero-propulsion use”, *J. Eur. Ceram. Soc.*, **22** (2002) 2757–2767.
12. M. Opeka, I.G. Talmy, E.J. Wuchina, J.A. Zaykoski, S.J. Causey, “Mechanical, thermal and oxidation properties of refractory hafnium and zirconium”, *J. Eur. Ceram. Soc.*, **19** (1999) 2405–2414.
13. S.M. Lakiza, J.S. Tyschenko, L.M. Lopato, “Phase diagram of the Al<sub>2</sub>O<sub>3</sub>-HfO<sub>2</sub>-Y<sub>2</sub>O<sub>3</sub> system”, *J. Eur. Ceram. Soc.*, **31** (2011) 1285–1291.
14. R. Licheri, R. Orru, A.M. Locci, G. Cao, “Efficient synthesis/sintering routes to obtain fully dense ultra-high-temperature ceramics (UHTCs)”, *Ind. Eng. Chem. Res.*, **46** (2007) 9087–9096.
15. M. Omori, “Sintering consolidation, reaction and crystal growth by the spark plasma system (SPS)”, *Mater. Sci. Eng. A*, **287** (2000) 183–188.
16. R.E. Hann, P.R. Suitch, J.L. Pentecost, “Monoclinic crystal structure of ZrO<sub>2</sub> and HfO<sub>2</sub> refined from X-ray powder diffraction data”, *J. Am. Ceram. Soc.*, **68** (1985) 285–286.
17. E.R. Andrievskaya, “Phase equilibria in the refractory oxide systems of zirconia hafnia and yttria with rare-earth oxides”, *J. Eur. Ceram. Soc.*, **28** (2008) 2363–2388.
18. M. Mann, J. Kolis, “Hydrothermal crystal growth of yttrium and rare earth stabilized hafnia”, *J. Cryst. Growth*, **312** (2010) 461–465.
19. M.R. Winter, D.R. Clarke, “Thermal conductivity of yttria-stabilized zirconia-hafnia solid solutions”, *Acta Mater.*, **54** (2006) 5051–5059.

20. B. Matović, D. Bučevac, M. Prekajski, V. Maksimović, D. Gautam, K. Yoshida, T. Yano, "Synthesis and characterization of nanometric yttrium-doped hafnia solid solutions", *J. Eur. Ceram. Soc.*, **32** (2012) 1971–1976.
21. P. Scherrer, "Bestimmung der Grösse und der inneren Struktur von Kolloidteilchen mittels Röntgenstrahlen", *Gött. Nachr.*, **2** (1918) 98–100.
22. K. Yoshida, K. Matsukawa, M. Imai, T. Yano, "Formation of carbon coating on SiC fiber for two-dimensional SiCf/SiC composites by electrophoretic deposition", *Mater. Sci. Eng. B*, **161** (2009) 188–192.
23. G. Fatjo, M. Hadfield, C. Vieillard, J. Sekulić, "Early stage cavitation erosion within ceramics - an experimental investigation", *Ceram. Int.*, **35** (2009) 3301–3312.
24. S. Martinović, M. Dojčinović, M. Dimitrijević, A. Devečerski, B. Matović, T. Volkov-Husović, "Implementation of image analysis on thermal shock and cavitation resistance testing of refractory concrete", *J. Eur. Ceram. Soc.*, **30** (2010) 3303–3309.
25. T. Okada, Y. Iwai, S. Hattori, N. Tanimura, "Relation between impact load and the damage produced by cavitation bubble collapse", *Wear*, **184** (1995) 231–239.
26. M. Dojčinović, T. Volkov-Husović, "Cavitation damage of the medium carbon steel: implementation of image analysis", *Mater. Lett.*, **62** (2008) 953–956.
27. G. Bregliozzi, A. di Schino, S.I.-U. Ahmed, J.M. Kenny, H. Haefke, "Cavitation wear behaviour of austenitic stainless steels with different grain sizes", *Wear*, **258** (2005) 503–510.